Historical changes in wind driven ocean circulation can accelerate global warming

Kay McMonigal[1], Sarah Larson[1], Shineng Hu[2], and Ryan Kramer[3,4]

[1] Department of Marine, Earth, and Atmospheric Sciences, North Carolina State University, Raleigh, NC, USA

[2] Division of Earth and Climate Sciences, Nicholas School of the Environment, Duke University, Durham, NC, USA

[3] Climate and Radiation Laboratory, Earth Sciences Division, NASA Goddard Space Flight Center, Greenbelt, MD, USA
[4] Goddard Earth Science Technology Research II, University of Maryland Baltimore County, Baltimore, MD, USA

Corresponding author: Kay McMonigal (ktmcmoni@ncsu.edu)

Key Points:

- Externally forced changes to wind driven ocean circulation accelerate global warming by 17% in a coupled climate model
- The Antarctic Circumpolar Current and Pacific ocean circulations are influenced by externally forced wind stress changes
- Externally forced changes to wind driven ocean circulation amplify Southern Hemisphere warming

Abstract

Mitigation and adaptation strategies for climate change depend on accurate climate projections for the coming decades. While changes in radiative heat fluxes are known to contribute to surface warming, changes to ocean circulation can also impact the rate of surface warming. Previous studies suggest that projected changes to ocean circulation reduce the rate of global warming. However, these studies consider large greenhouse gas forcing scenarios, which induce a significant buoyancy driven decline of the Atlantic Meridional Overturning Circulation (AMOC). Here, we use a climate model to quantify the previously unknown impact of changes to wind driven ocean circulation on global surface warming. Wind driven ocean circulation changes amplify the externally forced warming rate by 17% over 1979-2014. Accurately simulating changes to the atmospheric circulation is key to improving near term climate projections.

Plain Language Summary

Global warming of surface air temperature is largely due to increases in greenhouse gases, which lead to increased radiative heat fluxes towards Earth's surface. However, the exact pattern and rate of global warming is also influenced by the uptake and redistribution of heat by the ocean, which can be altered by warming. Previous studies have quantified the role of the changing ocean circulation as a whole on the rate and pattern of global warming. However, the relative contribution of different ocean dynamical processes has not been explored yet. Ocean circulation can broadly be divided components driven by wind and density differences. Here, we quantify the role of changes to the wind driven ocean circulation onto global air temperature warming. We find that changes to the wind driven ocean circulation amplify global warming by 17% over 1979-2014. Climate models need to adequately simulate changes to the winds, and the ocean's response to these wind changes, to accurately project climate change.

1 Introduction

Anthropogenic forcing is expected to alter the atmospheric circulation as a response to increased net absorbed radiative heat fluxes (Held & Soden, 2006; Lu et al., 2008; Vecchi & Soden, 2007). The adjustment of the atmospheric circulation to anthropogenic forcing can then impact the ocean circulation by altering winds or buoyancy fluxes, two major drivers of the large-scale ocean circulation. The large-scale ocean circulation plays a key role in setting the spatially varying pattern of sea surface temperature (SST) warming by redistributing the heat taken up by the ocean from increased downward heat flux (Banks & Gregory, 2006; Hu et al., 2020, 2022; Liu et al., 2018; Lyu et al., 2020). This pattern of SST warming can feed back onto the atmosphere through pattern dependent radiative feedbacks, largely linked to cloud-SST feedbacks (termed "the pattern effect"; (Armour, 2017; Armour et al., 2013; Dong et al., 2019, 2020; Rose et al., 2014; Stevens et al., 2016). Therefore, changes to the atmospheric circulation that drive a change in ocean circulation could alter the globally averaged rate of anthropogenic warming.

Externally forced changes to the atmospheric circulation, and the impacts of these changes onto the oceanic circulations, have already begun to occur over the historical record. The Southern Hemisphere midlatitude winds have increased over the past 4 decades (Thompson et al., 2011; Thompson & Solomon, 2002), altering the wind driven circulation in the South Indian and South Pacific subtropical gyres (Beal & Elipot, 2016; Lee et al., 2015; McMonigal et al., 2018, 2022; Palmer et al., 2004; Roemmich et al., 2007, 2016). In the tropical Pacific, the trade winds have increased in strength (M. H. England et al., 2014; Mcgregor et al., 2012; Merrifield et al., 2012; Timmermann et al., 2010), leading to cooling in the equatorial Pacific (Seager et al., 2022).

Previous studies have quantified the role of the ocean circulation on the rate of anthropogenic warming under high emissions scenarios, such as a doubling or quadrupling of CO_2 (Garuba et al., 2018; Trossman et al., 2016; Winton et al., 2013). In these scenarios, the projected decline of the Atlantic Meridional Overturning Circulation (AMOC) dominates the oceanic response of the climate system, by cooling the high latitude North Atlantic and allowing for increased deep ocean heat uptake within the North Atlantic (Rugenstein et al., 2013). This leads to a decrease in the globally averaged surface warming, thus the overall role of the ocean is to mediate the surface warming rate. Beyond the impacts from AMOC decline, whether externally forced changes in the wind driven ocean circulation mediate or amplify the warming rate is relatively unexplored despite its potential influence on regional scales. Moreover, developing mitigation and adaptation strategies relies on accurate near term (20-40 year) climate projections (Hewitt & Lowe, 2018; Nissan et al., 2019), a timescale over which large AMOC trends are not expected (Lobelle et al., 2020; Weijer et al., 2020).

In this study, we quantify the role of externally forced changes to the wind driven ocean over 1979-2014 in the Community Earth System Model version 2 (CESM2). We isolate this effect by comparing two large ensembles within CESM2: one including the role of changes to the wind driven ocean circulation, and the other excluding it. Crucially, the effect of changes in the wind driven ocean circulation is opposite in sign to the role of ocean circulation on global warming under higher emission scenarios (Garuba et al., 2018; Trossman et al., 2016; Winton et al., 2013). This implies that the role of the changing ocean circulation on the globally averaged rate of surface warming depends on the ocean dynamics at play, with opposing roles of boundary driven ocean circulation changes like AMOC, and wind driven ocean circulation changes.

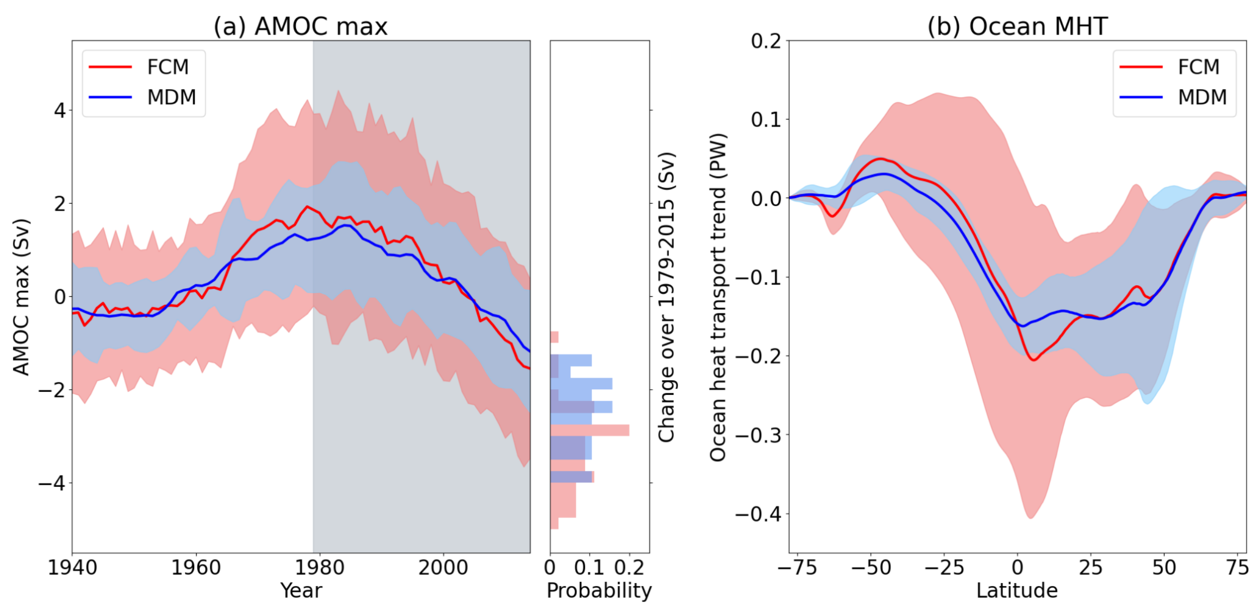

Fig. 1

(a) Ensemble mean AMOC intensity in each simulation (thick lines) with two standard deviation shading. Histogram shows trends over 1979-2014 in each ensemble member. (b) Ensemble mean trends in ocean meridional heat transport (MHT; thick lines) with two stand deviation shading.

2 Method

2.1 Experimental design

We use two CESM2 ensembles forced by realistic, time-varying 1850-2014 external forcing, including greenhouse gasses, anthropogenic aerosol emissions, natural aerosols (e.g. volcanic), and solar irradiance. In the first ensemble, referred to as FCM for "Fully Coupled Model", the ocean and atmosphere exchange time varying buoyancy and wind stress (momentum) fluxes. In the second ensemble, referred to as MDM for "Mechanically Decoupled Model", the ocean and atmosphere exchange time varying buoyancy fluxes but the ocean is forced by a fixed wind stress climatology, calculated from pre-industrial conditions. The atmospheric winds in MDM vary in time; only the wind stress forcing onto the ocean is fixed to a climatology. Both models have similar pre-industrial mean climates and ocean circulation (Figure S1, S2, S3). Additionally, because the low frequency, interhemispheric component of AMOC is predominantly buoyancy forced (Biastoch et al., 2008; Medhaug et al., 2012; Polo et al., 2014; Yeager & Danabasoglu, 2014), FCM and MDM simulate similar AMOC mean states (Larson et al., 2020), similar externally forced declines in AMOC (Fig. 1a), and similar externally forced trends in ocean meridional heat transport (Fig. 1b).

To isolate the externally forced trends, we compute the ensemble mean linear trends in each simulation to remove the internal variability (Bengtsson & Hodges, 2019; Deser et al., 2012, 2020; Hawkins et al., 2016; Machete & Smith, 2016). The difference between the ensemble mean trends in the FCM and MDM isolates climate changes due to externally forced trends in the wind driven ocean circulation. We refer to this component of the trends as due to the dynamic response of the ocean to changes in the "Winds", as we expect the total forced trend to be a linear superposition of wind and buoyancy forced trends (Fyfe et al., 2007; Yeager & Danabasoglu, 2014). In this coupled model set up, ocean circulation trends can feedback onto the atmosphere, sea ice, and land.

2.2 Model ensembles

Both FCM and MDM ensembles were run using the smoothed biomass burning set up of the Community Earth System Model version 2 (CESM2; (Danabasoglu et al., 2020; Fasullo et al., 2022; Rodgers et al., 2021). This model consists of the Community Atmosphere Model version 6, the Parallel Ocean Project version 2 (Smith et al., 2010), the Community Land Model version 5 (Lawrence et al., 2019), and the Los Alamos Community Ice CodE version 5 (Hunke et al., 2017). The model components communicate through the Common Infrastructure for Modeling the Earth (CIME) coupler. The alteration of the wind stress forcing passed to the ocean in the MDM ensemble is done within CIME, by overwriting the time varying wind stress forcing passed from the atmosphere to the ocean. Both models were forced by realistic 1850-2014 greenhouse gas emissions.

CESM2 is a part of CMIP6. In CMIP6, stratospheric ozone trends are prescribed, but no tropospheric ozone trends are included (Liu et al., 2022). Anthropogenic aerosols are prescribed, and lead to a SST cooling that is similar in structure to the greenhouse gas induced warming (Xie et al., 2013) but show distinct regional patterns in surface wind trends (Wang et al., 2016). CESM2 has a horizontal ocean resolution of approximately 1°.

The FCM ensemble was created by branching 50 ensemble members from a spun up, pre industrial model run for more than 1000 years. This includes 10 macro ensemble members, where each of the members is branched from a different pre industrial climate state, and 4 sets of 10 micro ensemble members, where each set of micro ensemble members are branched from a different pre industrial climate, and each ensemble member is created by adding a random, round off error level perturbation to the atmospheric potential temperature field.

The MDM ensemble was created by branching 20 ensemble members from a spun up, pre industrial MDM model run. The wind stress climatology forcing in the MDM runs was calculated from 50 years of the FCM preindustrial run. Each ensemble member was branched from a different year of the preindustrial MDM run, making it a macro ensemble.

The FCM and MDM pre industrial runs have similar mean states. In the pre industrial run, sea surface temperatures are warmer and mixed layer depths are shallower in MDM (Fig. S1, S2). The ocean circulation mean state is similar in the two models, in all regions except the Southern Ocean (Fig. S3). MDM has a stronger Antarctic Circumpolar Current, likely due to alterations of the isopycnals across the Southern Ocean.

2.3 Observational data

For comparison to the modeled trends, observational trends were estimated by using GISS Surface Temperature Anomaly version 4 (GISTEMP) surface air temperature and ECMWF reanalysis version 5 (ERA5) wind stress.

2.4 Analyses

To analyze the globally averaged surface temperature response, we consider the ensemble mean reference height air temperature. AMOC max is calculated as the maximum AMOC streamfunction between 20° and 65°N, at each time step. All trends shown are linear trends calculated from annual mean anomalies from the climatology calculated over 1941-1970 period, to remove any dependence on mean state differences. Trends are multiplied by the length of the time period, to give units that match the variable of interest. Top of atmosphere total radiation, longwave radiation, and shortwave radiation are defined as positive downward. For the radiative flux regressions shown in Fig. S10, the earlier time period trends are calculated as the linear trends over 1966-1987, excluding 1975, 1982, and 1983. This is due to large volcanic influence during the three excluded years. The later time period trends are calculated as the linear trends over 1996-2014, to avoid the large volcanic influence of Mt. Pinatubo in 1991.

2.5 Significance testing

To determine the regions and time periods where trends are significantly different, we consider the spread of the ensemble members as a normal distribution. To test if the distributions are significantly different, we calculate the Z statistic and use 95% significance ($Z>=1.96$) as a threshold, where:

$$Z = \frac{X_{FCM} - X_{MDM}}{\sqrt[2]{\sigma_{FCM}^2 - \sigma_{MDM}^2}}$$

X is the ensemble mean from each simulation. $\boldsymbol{\sigma}$ is the standard deviation of each ensemble member divided by the square root of the number of ensemble members.

The global mean temperature difference is also significant at the 95% level when considering temporal correlations of residuals of the difference of ensemble means, following (Santer et al., 2000).

3 Wind stress and wind driven ocean circulation trends

Externally forced changes to the wind stress primarily manifest within the Southern Hemisphere westerlies and the Pacific trades and North Pacific westerlies (Fig. 2a). The Southern Hemisphere westerlies strengthen and shift poleward beginning in 1970 (Fig. S4) and broadly agree with reanalysis wind stress trends in the region (Fig. S5). The strengthening and shifting of the Southern Hemishere westerlies has been linked to both stratospheric ozone and greenhouse gas forcing (Thompson et al., 2011; Thompson & Solomon, 2002). The Pacific trades and North Pacific westerlies weaken beginning in 1990 (Fig. S4). The weakening of the Pacific trades is inconsistent with reanalyses (M. H. England et al., 2014; Mcgregor et al., 2012; Merrifield et al., 2012; Timmermann et al., 2010), while the weakening of the North Pacific westerlies broadly matches the reanalysis trend (Fig. S5).

These wind stress trends lead to externally forced changes in the horizontal barotropic ocean circulation (BSF) over 1979-2014 (Fig. 2c; mean barotropic streamfunction shown in Fig. S6). The Antarctic Circumpolar Current accelerates due to wind stress trends, in agreement with the observed acceleration of Antarctic Circumpolar Current velocities (Shi et al., 2021). The tropical and North Pacific circulations weaken. Trends in the barotropic circulation are generally similar to trends in ocean currents averaged over the upper 150 m (Fig. S7).

Comparing the role of buoyancy (illustrated by the MDM trend) and wind stress forcing (illustrated by Winds trend) on externally forced changes in the BSF shows that buoyancy forcing dominates the changes in the Atlantic Ocean (Fig. 2b,c). The buoyancy forced weakening of the North Atlantic circulation is consistent with the simulated decline in the interhemispheric AMOC in the model (Fig. 1a). Although the simulated AMOC decline is similar in both models, a significantly larger decline of 3.5 Sv is seen in FCM, while MDM simulates a decline of 2.6 Sv. This suggests that, although buoyancy forcing dominates the forced AMOC decline, the changes in surface wind stress act to enhance the AMOC decline by about 25%. Both buoyancy and wind stress changes contribute to a weakening of the South Indian Ocean subtropical gyre. This is the opposite sign of the observed strengthening of the Southern Hemisphere gyres (McMonigal et al., 2018; Palmer et al., 2004; Roemmich et al., 2007, 2016), suggesting that the model may be biased or low frequency internal variability projects onto the observed trends. Both buoyancy and wind stress changes contribute to changes in the Antarctic Circumpolar Current strength, although with opposite signs. Wind stress changes accelerate the Antarctic Circumpolar Current, while buoyancy changes slightly weaken it. This is opposite to the role of buoyancy forcing found under stronger greenhouse gas forcing (Peng et al., 2022; SHI et al., 2020). This suggests that the response of the Southern Ocean to buoyancy forcing may depend on timescale or magnitude of forcing.

Overall, the modeled externally forced acceleration of the Antarctic Circumpolar Current due to changes in the overlying westerlies is in agreement with atmospheric and oceanic observations. The weakening of the Pacific circulations due to weakening of the overlying winds is not corroborated by atmospheric reanalyses.

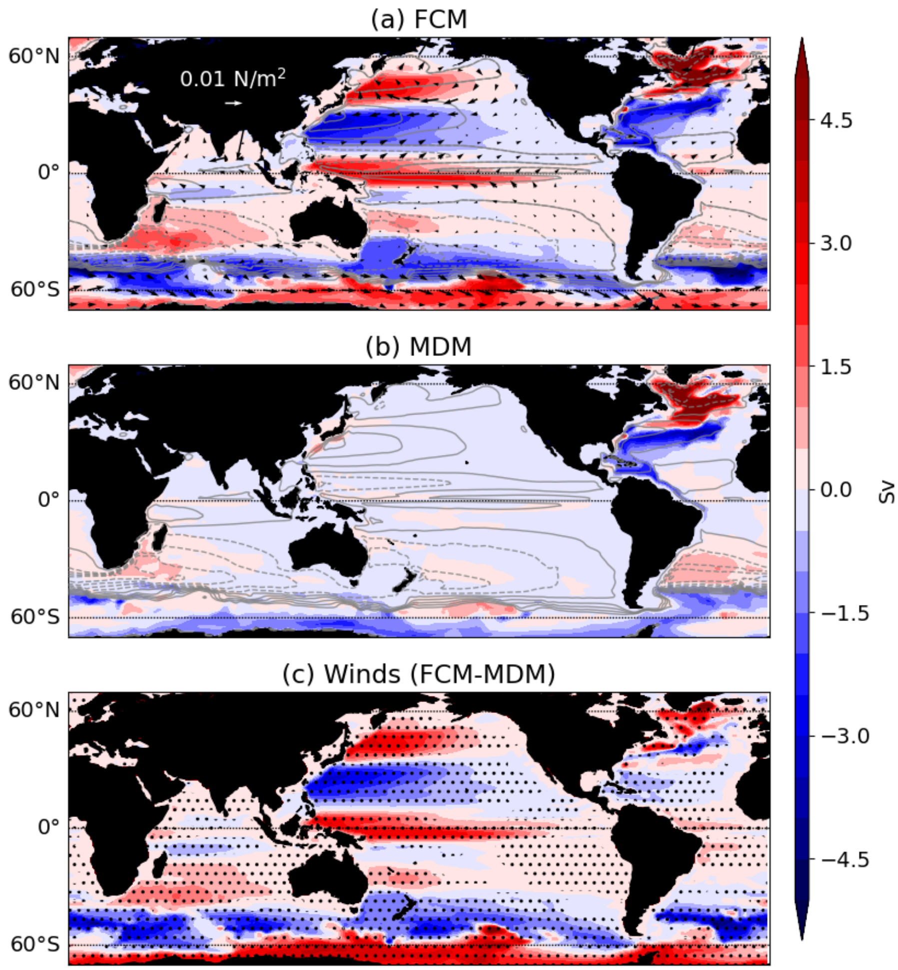

Fig. 2
(a) Trend in FCM ensemble mean barotropic streamfunction (BSF) over 1979-2014 (colored contours) and wind stress (arrows). Gray contours show the 1941-1970 mean BSF, with contour values every 15 Sv from -75 Sv to 60 Sv. (b) Trend in MDM ensemble mean barotropic streamfunction over 1979-2014 (colored contours) and wind stress (arrows). Gray contours show the 1941-1970 mean BSF, with contour values every 15 Sv from -75 Sv to 60 Sv. (c) Winds ensemble mean trends. Stippling shows where FCM and MDM ensemble mean trends are significantly different. For all panels, negative values indicating counterclockwise circulation are dashed and positive values indicating clockwise circulation are solid.

4 Wind driven ocean circulation trend feedbacks

Global mean surface temperature anomalies are very similar with and without wind driven ocean circulation changes, until the 1970s (Fig. 3a). Trends in the wind stress forcing on the ocean lead to statistically significant global mean surface warming differences in the early 1990s (Fig. 3b). This is several decades after changes in the Southern Ocean winds, and temporally aligned with changes to the Pacific trade winds (Fig. S4). Changes to the wind stress driven ocean circulation lead to increased global warming of 0.15°C, or 17% of the trend in FCM (Table S1). The observed rate of global surface temperature change (0.59°C) is within the range of the MDM ensemble and is slightly colder than the range of possibilities simulated by the FCM ensemble. To understand the cause of the amplified warming in FCM compared to MDM, we first focus on the differences in the warming patterns between the two simulations.

Changes in the wind driven ocean circulation lead to more warming over the Southern Hemisphere and the eastern tropical Pacific (Fig. 4d). In both regions, models commonly show too much warming as compared to observations (Fan et al., 2014; Seager et al., 2022; Turner et al., 2013). In these regions, the MDM simulation shows better agreement with observations as compared to the more realistic FCM simulation, suggesting that a component of the model biases could be due to incorrect wind stress trends or incorrect ocean response to wind stress trends. In the Northern Hemisphere, trends in wind stress forcing shift warming patterns, including a zonal shift of the North Atlantic warming hole and a meridional shift of the simulated location of maximum warming in the North Pacific. Trends in wind stress forcing also significantly alter surface temperature trends over land, leading to a faster warming rate over much of the Americas, Europe, Africa, and Australia and slower warming over parts of Asia.

As an initial assessment of the dynamics leading to the warming pattern in Winds, we compare the surface air temperature trend (Fig. 4d) to the upper 2000 m ocean heat content (OHC) trend (Fig. S8c) and the mixed layer depth trend (Fig. S9c). Changes to the wind driven ocean circulation lead to more OHC warming (greater surface heat fluxes into the ocean) in the Southern Hemisphere, North Atlantic, and high latitude North Pacific, and less OHC warming (surface heat fluxes out of the ocean) in the tropical Pacific. In the zonal mean, heat flux into the ocean is larger in FCM than MDM in the subtropics, while near the equator, FCM has surface heat fluxes out of the ocean while MDM has surface heat fluxes into the ocean (Fig. S10a). Changes to the wind driven ocean circulation lead to a deeper mixed layer depths in the Southern Ocean and high latitude North Atlantic. Therefore, in the Southern Ocean, warmer surface temperatures in Winds are collocated with regions of larger OHC warming (Fig. S8) and deeper mixed layers (Fig. S9), suggesting that atmospheric processes may dominate. In contrast, in the tropical Pacific, Winds shows amplified air temperature warming, reduced OHC warming, surface heat fluxes out of the ocean, and an altered mixed layer depth gradient across the basin (Fig. S8,S9). This suggests that dynamic oceanic processes dominate the wind driven warming seen in the Pacific. Further study using regional heat budgets will elucidate specific dynamics at play.

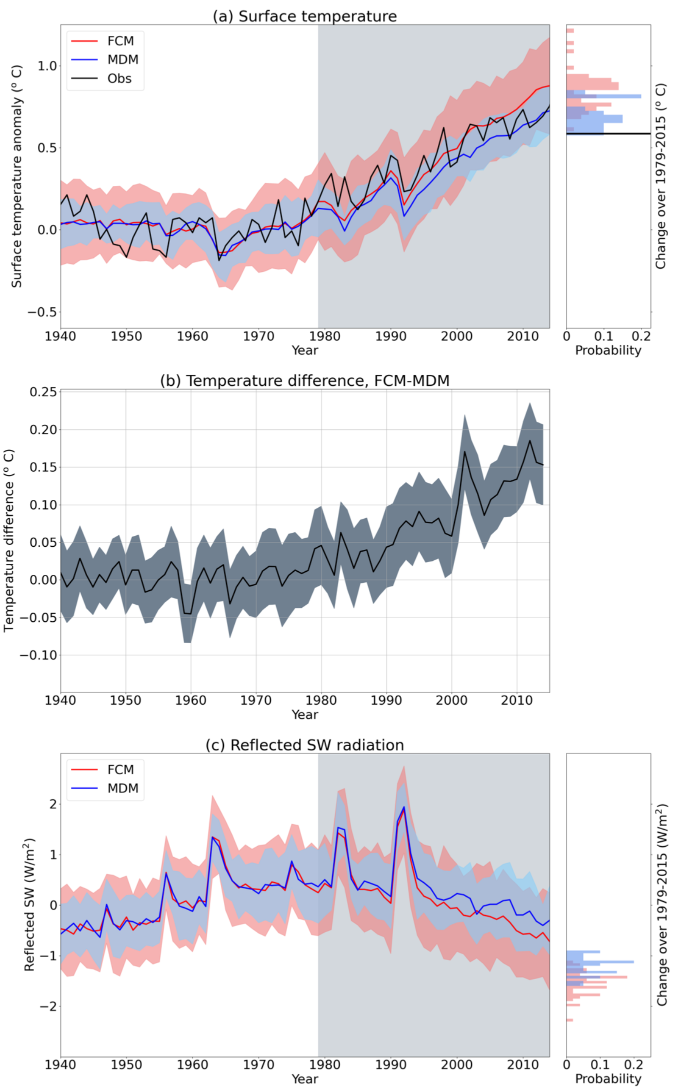

Fig. 3

(a) Surface air temperature anomalies, with red showing FCM and blue showing MDM. Thick lines are ensemble means. Shading shows 2 standard deviations across ensemble members. Thick black line shows the GISTEMP observational product. Right-hand side histograms show the trend over 1979-2015 multiplied by the time period, to yield the change of each field. (b) The FCM-MDM temperature difference, with shading showing the 95% confidence interval. (c) Same as (a) but for global mean all sky top of atmosphere upward shortwave radiation anomalies.

The different warming patterns in each simulation could drive the different globally averaged warming rates through ocean heat uptake differences, or through differences in radiative feedbacks which alter the top of atmosphere radiation balance. Specifically, when comparing two simulations with the same external forcing, the simulation with a faster global warming rate must either have smaller ocean heat uptake or larger net radiative energy absorption by the planet (i.e. a larger top of atmosphere radiation imbalance) than the simulation with a slower global warming rate. The zonally averaged ocean heat uptake patterns in FCM and MDM are different, especially in the tropics where FCM takes up less heat than MDM (Fig.

S10a), which likely plays a role in the different zonal mean rates of surface warming (Fig. S10b) and differing values of ocean heat uptake efficiency (Table S1). Globally averaged, however, FCM warms more than MDM while also taking up more heat into the ocean (Table S1). Therefore, ocean heat uptake cannot explain the amplified warming in FCM. Instead, radiative fluxes, which are known to be dependent on the pattern of surface warming, lead to the amplification of the globally averaged warming rate in FCM. FCM begins to warm faster than MDM in about 1990 (Fig. 3c), and so we focus the next analyses on the period 1995-2014.

Over 1995-2014, the all-sky, top of atmosphere (TOA) radiation imbalance in FCM increases at a faster rate than in MDM (Fig. S10c), signifying the planet is gaining radiative energy at a faster rate in FCM than in MDM. This increase in radiative energy occurs in shortwave radiation under all-sky conditions but not in clear-sky conditions (Fig. S10f) nor in longwave radiation under all-sky conditions (Fig. S10e), suggesting shortwave cloud radiative effects explain the difference in the overall net radiative trends between FCM and MDM. In context of the different SST warming patterns between the simulations, we expect to see different net radiative trends. The amplified warming beginning in 1995 is consistent with when the Pacific trades weaken in FCM, leading to increased warming in the eastern equatorial Pacific (Fig. 4d) through ocean dynamical processes. Anomalous SST warming in the eastern tropical Pacific is known to decrease the lower tropospheric stability and reduce low clouds locally (Andrews et al., 2015; Andrews & Webb, 2018; Ceppi & Gregory, 2017; Zhou et al., 2017), thereby reducing the global reflected shortwave radiation (Fig. 3c) and resulting in an increased downward top of atmosphere radiation imbalance (Fig. S10c). These results suggests that the weakening of the Pacific trades may play a larger role than the poleward intensified Southern Hemisphere westerlies in the amplification of global surface warming in FCM. However, it is possible that regional warming differences in the Southern Hemisphere are more impacted by the Southern Hemisphere westerly changes than the Pacific trade changes. Additionally, the Southern Hemisphere westerly wind shift and the weakened Pacific trades could be indirectly linked through an extratropical to tropical teleconnection (Dong et al., 2022; M. R. England et al., 2020).

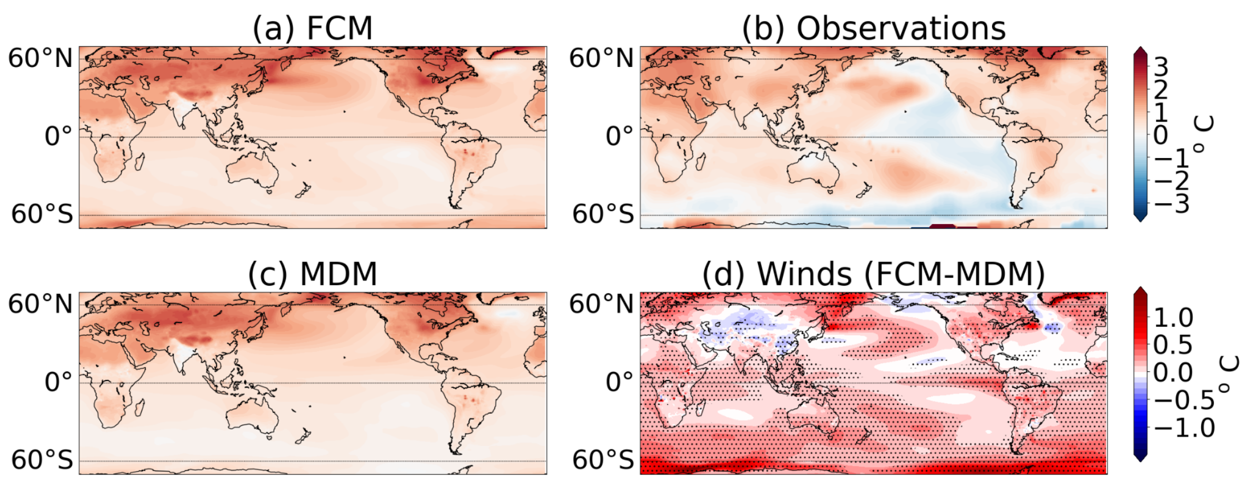

Fig. 4
(a) Ensemble mean trend in surface air temperature over 1979-2014 in FCM. (b) Same but for GISTEMP observational product (c) Same but for MDM. (d) Same but for Winds. Stippling in bottom right is where FCM and MDM ensemble means are statistically different.

5 Conclusions

Our study demonstrates that the wind driven ocean circulation plays a critical role in pacing the global warming rate over 1979-2014 in a CMIP6 model, under realistic greenhouse gas and aerosol forcing. Externally forced changes to the wind driven ocean circulation lead to increased surface warming of 0.15°C (17%). This increased warming is distributed as amplified warming over most of the Southern Hemisphere and a shifting of warming patterns in the Northern Hemisphere. The increased rate of warming caused by trends in wind driven ocean is opposite in sign to the decreased rate of global warming due to ocean circulation changes found in previous studies (Garuba et al., 2018; Trossman et al., 2016; Winton et al., 2013). We hypothesize that this discrepancy is due to the different role of the AMOC decline, which dominates in studies that use large greenhouse gas forcings, and wind driven ocean circulation changes which are isolated in our experimental set up. This suggests that the role of ocean circulation changes on global surface warming are dependent on dynamics and that at any point in time, the competing effects of an AMOC decline driven cooling and a wind driven ocean circulation warming dictate the total role of ocean circulation changes on surface warming. If this hypothesis is correct, ocean circulation changes could be contributing to time variability in the climate feedback parameter (Andrews et al., 2015). Over long time periods, AMOC decline likely dominates the oceanic warming feedback, and reduces global surface warming, whereas over shorter time scales (like those investigated here), wind driven ocean circulation changes can amplify surface warming.

Wind driven ocean circulation changes amplify SST warming in the eastern tropical Pacific, which feeds back onto the top of atmosphere radiation imbalance and leads to amplified global surface warming. What this means for the climate system depends on whether the wind stress trends in coupled models are systematically biased. Coupled climate models commonly simulate inaccurate SST trends in the eastern tropical Pacific (Seager et al., 2019, 2022), which can lead to global biases through cloud-SST feedback (Dong et al., 2021). Under this interpretation, biased wind stress trends or an incorrectly simulated oceanic response to the wind stress trends may be driving an overestimate of the rate of global surface warming. On the other hand, it is possible that the model-bias mismatch in the eastern tropical Pacific is due to natural variability, which offsets the forced trend isolated by model ensembles (Bordbar et al., 2017; Olonscheck et al., 2020; Watanabe et al., 2021). This interpretation would imply that the role of wind driven ocean circulation changes could amplify the surface warming rate, once the eastern tropical Pacific internal variability changes phases. In either case, it is crucial to understand climate model behavior to ensure future climate model projections are accurate.

Acknowledgments

We thank Nan Rosenbloom for assistance running the MDM ensemble, and Clara Deser and the organizers of CLIVAR pattern effect meeting for productive scientific discussions. This work is supported by NSF Grant AGS-1951713 (KM and SML) and NASA Grant 80NSSC22K1025 (SH). RK was supported by NOAA award NA18OAR4310269 and NASA grant no. 80NSSC21K1968. We also acknowledge the high-performance computing support from Cheyenne provided by NCAR's Computing and Information Services Lab, sponsored by NSF.

Open Research

CESM2 FCM output is available from the Earth System Grid Federation (ESGF; at https://esgf-node.llnl.gov/search/cmip6/) as part of the CESM2 Large Ensemble (LENS2; https://www.cesm.ucar.edu/projects/community-projects/LENS2/). GISTEMP output was obtained freely from the National Aeronautics and Space Administration (NASA) Goddard Institute for Space Studies (https://data.giss.nasa.gov/gistemp/). ERA5 output was obtained freely from the European Centre for Medium-Range Weather Forecasts (ECMWF; https://www.ecmwf.int/en/forecasts/dataset/ecmwf-reanalysis-v5). Data analyzed from the CESM2 MDM are available in the Zenodo data repository at https://doi.org/10.5281/zenodo.7154374. CESM2 MDM model source code changes and wind stress climatology forcing datasets are available in the Zenodo data repository at https://doi.org/10.5281/zenodo.6678286. Code to make the figures is available in the Zenodo data repository at 10.5281/zenodo.7158684.

References

Andrews, T., Gregory, J. M., & Webb, M. J. (2015). The Dependence of Radiative Forcing and Feedback on Evolving Patterns of Surface Temperature Change in Climate Models. *Journal of Climate*, *28*(4), 1630–1648. https://doi.org/10.1175/JCLI-D-14-00545.1

Andrews, T., & Webb, M. J. (2018). The Dependence of Global Cloud and Lapse Rate Feedbacks on the Spatial Structure of Tropical Pacific Warming. *Journal of Climate*, *31*(2), 641–654. https://doi.org/10.1175/JCLI-D-17-0087.1

Armour, K. C. (2017). Energy budget constraints on climate sensitivity in light of inconstant climate feedbacks. *Nature Climate Change*, *7*(5), 331–335. https://doi.org/10.1038/nclimate3278

Armour, K. C., Bitz, C. M., & Roe, G. H. (2013). Time-Varying Climate Sensitivity from Regional Feedbacks. *Journal of Climate*, *26*(13), 4518–4534. https://doi.org/10.1175/JCLI-D-12-00544.1

Banks, H. T., & Gregory, J. M. (2006). Mechanisms of ocean heat uptake in a coupled climate model and the implications for tracer based predictions of ocean heat uptake. *Geophysical Research Letters*, *33*(7). https://doi.org/10.1029/2005GL025352

Beal, L. M., & Elipot, S. (2016). Broadening not strengthening of the Agulhas Current since the early 1990s. *Nature*, *540*(7634), Article 7634. https://doi.org/10.1038/nature19853

Bengtsson, L., & Hodges, K. I. (2019). Can an ensemble climate simulation be used to separate climate change signals from internal unforced variability? *Climate Dynamics*, *52*(5), 3553–3573. https://doi.org/10.1007/s00382-018-4343-8

Biastoch, A., Böning, C. W., Getzlaff, J., Molines, J.-M., & Madec, G. (2008). Causes of Interannual–Decadal Variability in the Meridional Overturning Circulation of the Midlatitude North Atlantic Ocean. *Journal of Climate*, *21*(24), 6599–6615. https://doi.org/10.1175/2008JCLI2404.1

Bordbar, M. H., Martin, T., Latif, M., & Park, W. (2017). Role of internal variability in recent decadal to multidecadal tropical Pacific climate changes. *Geophysical Research Letters*, *44*(9), 4246–4255. https://doi.org/10.1002/2016GL072355

Ceppi, P., & Gregory, J. M. (2017). Relationship of tropospheric stability to climate sensitivity and Earth's observed radiation budget. *Proceedings of the National Academy of Sciences*, *114*(50), 13126–13131. https://doi.org/10.1073/pnas.1714308114

Danabasoglu, G., Lamarque, J. F., Bacmeister, J., Bailey, D. A., DuVivier, A. K., Edwards, J., Emmons, L. K., Fasullo, J., Garcia, R., Gettelman, A., Hannay, C., Holland, M. M., Large, W. G., Lauritzen, P. H., Lawrence, D. M., Lenaerts, J. T. M., Lindsay, K., Lipscomb, W. H., Mills, M. J., … Strand, W. G. (2020). The Community Earth System Model Version 2 (CESM2). *Journal of Advances in Modeling Earth Systems*, *12*(2), 1–35. https://doi.org/10.1029/2019MS001916

Deser, C., Lehner, F., Rodgers, K. B., Ault, T., Delworth, T. L., DiNezio, P. N., Fiore, A., Frankignoul, C., Fyfe, J. C., Horton, D. E., Kay, J. E., Knutti, R., Lovenduski, N. S., Marotzke, J., McKinnon, K. A., Minobe, S., Randerson, J., Screen, J. A., Simpson, I. R., & Ting, M. (2020). Insights from Earth system model initial-condition large ensembles and future prospects. *Nature Climate Change*, *10*(4), Article 4. https://doi.org/10.1038/s41558-020-0731-2

Deser, C., Phillips, A., Bourdette, V., & Teng, H. (2012). Uncertainty in climate change projections: The role of internal variability. *Climate Dynamics*, *38*(3–4), 527–546. https://doi.org/10.1007/s00382-010-0977-x

Dong, Y., Armour, K. C., Battisti, D. S., & Blanchard-Wrigglesworth, E. (2022). Two-way teleconnections between the Southern Ocean and the tropical Pacific via a dynamic feedback. *Journal of Climate*, 1–37. https://doi.org/10.1175/JCLI-D-22-0080.1

Dong, Y., Armour, K. C., Proistosescu, C., Andrews, T., Battisti, D. S., Forster, P. M., Paynter, D., Smith, C. J., & Shiogama, H. (2021). Biased Estimates of Equilibrium Climate Sensitivity and Transient Climate Response Derived From Historical CMIP6 Simulations. *Geophysical Research Letters*, *48*(24), e2021GL095778. https://doi.org/10.1029/2021GL095778

Dong, Y., Armour, K. C., Zelinka, M. D., Proistosescu, C., Battisti, D. S., Zhou, C., & Andrews, T. (2020). Intermodel Spread in the Pattern Effect and Its Contribution to Climate Sensitivity in CMIP5 and CMIP6 Models. *Journal of Climate*, *33*(18). https://journals.ametsoc.org/view/journals/clim/33/18/jcliD191011.xml

Dong, Y., Proistosescu, C., Armour, K. C., & Battisti, D. S. (2019). Attributing Historical and Future Evolution of Radiative Feedbacks to Regional Warming Patterns using a Green's Function Approach: The Preeminence of the Western Pacific. *Journal of Climate*, *32*(17), 5471–5491. https://doi.org/10.1175/JCLI-D-18-0843.1

England, M. H., Mcgregor, S., Spence, P., Meehl, G. A., Timmermann, A., Cai, W., Gupta, A. S., Mcphaden, M. J., Purich, A., & Santoso, A. (2014). Recent intensification of wind-driven circulation in the Pacific and the ongoing warming hiatus. *Nature Climate Change*, *4*(3), 222–227. https://doi.org/10.1038/nclimate2106

England, M. R., Polvani, L. M., Sun, L., & Deser, C. (2020). Tropical climate responses to projected Arctic and Antarctic sea-ice loss. *Nature Geoscience*, *13*(4), 275–281. https://doi.org/10.1038/s41561-020-0546-9

Fan, T., Deser, C., & Schneider, D. P. (2014). Recent Antarctic sea ice trends in the context of Southern Ocean surface climate variations since 1950. *Geophysical Research Letters*, *41*(7), 2419–2426. https://doi.org/10.1002/2014GL059239

Fasullo, J. T., Lamarque, J.-F., Hannay, C., Rosenbloom, N., Tilmes, S., DeRepentigny, P., Jahn, A., & Deser, C. (2022). Spurious Late Historical-Era Warming in CESM2 Driven by Prescribed Biomass Burning Emissions. *Geophysical Research Letters*, *49*(2), e2021GL097420. https://doi.org/10.1029/2021GL097420

Fyfe, J. C., Saenko, O. A., Zickfeld, K., Eby, M., & Weaver, A. J. (2007). The role of poleward-intensifying winds on Southern Ocean warming. *Journal of Climate*, *20*(21), 5391–5400. https://doi.org/10.1175/2007JCLI1764.1

Garuba, O. A., Lu, J., Liu, F., & Singh, H. A. (2018). The Active Role of the Ocean in the Temporal Evolution of Climate Sensitivity. *Geophysical Research Letters*, *45*(1), 306–315. https://doi.org/10.1002/2017GL075633

Hawkins, E., Smith, R. S., Gregory, J. M., & Stainforth, D. A. (2016). Irreducible uncertainty in near-term climate projections. *Climate Dynamics*, *46*(11), 3807–3819. https://doi.org/10.1007/s00382-015-2806-8

Held, I. M., & Soden, B. J. (2006). Robust Responses of the Hydrological Cycle to Global Warming. *Journal of Climate*, *19*(21), 5686–5699. https://doi.org/10.1175/JCLI3990.1

Hewitt, C. D., & Lowe, J. A. (2018). Toward a European Climate Prediction System. *Bulletin of the American Meteorological Society*, *99*(10), 1997–2001. https://doi.org/10.1175/BAMS-D-18-0022.1

Hu, S., Xie, S. P., & Kang, S. M. (2022). Global Warming Pattern Formation: The Role of Ocean Heat Uptake. *Journal of Climate*, *35*(6), 1885–1899. https://doi.org/10.1175/JCLI-D-21-0317.1

Hu, S., Xie, S. P., & Liu, W. (2020). Global pattern formation of net ocean surface heat flux response to greenhouse warming. *Journal of Climate*, *33*(17), 7503–7522. https://doi.org/10.1175/JCLI-D-19-0642.1

Hunke, E., Lipscomb, W., Jones, P., Turner, A., Jeffery, N., & Elliott, S. (2017). *CICE, The Los Alamos Sea Ice Model* (CICE; 005315WKSTN00). Los Alamos National Lab. (LANL), Los Alamos, NM (United States). https://www.osti.gov/biblio/1364126

Larson, S. M., Buckley, M. W., & Clement, A. C. (2020). Extracting the buoyancy-driven atlantic meridional overturning circulation. *Journal of Climate*, *33*(11), 4697–4714. https://doi.org/10.1175/JCLI-D-19-0590.1

Lawrence, D. M., Fisher, R. A., Koven, C. D., Oleson, K. W., Swenson, S. C., Bonan, G., Collier, N., Ghimire, B., van Kampenhout, L., Kennedy, D., Kluzek, E., Lawrence, P. J., Li, F., Li, H., Lombardozzi, D., Riley, W. J., Sacks, W. J., Shi, M., Vertenstein, M., … Zeng, X. (2019). The Community Land Model Version 5: Description of New Features, Benchmarking, and Impact of Forcing Uncertainty. *Journal of Advances in Modeling Earth Systems*, *11*(12), 4245–4287. https://doi.org/10.1029/2018MS001583

Lee, S.-K., Park, W., Baringer, M. O., Gordon, A. L., Huber, B., & Liu, Y. (2015). Pacific origin of the abrupt increase in Indian Ocean heat content during the warming hiatus. *Nature Geoscience*, *8*(May), 445–449. https://doi.org/10.1038/ngeo2438

Liu, W., Hegglin, M. I., Checa-Garcia, R., Li, S., Gillett, N. P., Lyu, K., Zhang, X., & Swart, N. C. (2022). Stratospheric ozone depletion and tropospheric ozone increases drive Southern Ocean interior warming. *Nature Climate Change*, *12*(4), Article 4. https://doi.org/10.1038/s41558-022-01320-w

Liu, W., Lu, J., Xie, S.-P., Fedorov, A., Liu, W., Lu, J., Xie, S.-P., & Fedorov, A. (2018). Southern Ocean heat uptake, redistribution and storage in a warming climate: The role of meridional overturning circulation. *Journal of Climate*, JCLI-D-17-0761.1. https://doi.org/10.1175/JCLI-D-17-0761.1

Lobelle, D., Beaulieu, C., Livina, V., Sévellec, F., & Frajka-Williams, E. (2020). Detectability of an AMOC Decline in Current and Projected Climate Changes. *Geophysical Research Letters*, *47*(20), e2020GL089974. https://doi.org/10.1029/2020GL089974

Lu, J., Chen, G., & Frierson, D. M. W. (2008). Response of the Zonal Mean Atmospheric Circulation to El Niño versus Global Warming. *Journal of Climate*, *21*(22), 5835–5851. https://doi.org/10.1175/2008JCLI2200.1

Lyu, K., Zhang, X., Church, J. A., & Wu, Q. (2020). Processes responsible for the southern hemisphere ocean heat uptake and redistribution under anthropogenic warming. *Journal of Climate*, *33*(9), 3787–3807. https://doi.org/10.1175/JCLI-D-19-0478.1

Machete, R. L., & Smith, L. A. (2016). Demonstrating the value of larger ensembles in forecasting physical systems. *Tellus A: Dynamic Meteorology and Oceanography*, *68*(1), 28393. https://doi.org/10.3402/tellusa.v68.28393

Mcgregor, S., Gupta, A. S., & England, M. H. (2012). Constraining wind stress products with sea surface height observations and implications for Pacific Ocean sea level trend attribution. *Journal of Climate*, *25*(23), 8164–9176. https://doi.org/10.1175/JCLI-D-12-00105.1

McMonigal, K., Beal, L. M., & Willis, J. K. (2018). The Seasonal Cycle of the South Indian Ocean Subtropical Gyre Circulation as Revealed by Argo and Satellite Data. *Geophysical Research Letters*, *45*(17), 9034–9041. https://doi.org/10.1029/2018GL078420

McMonigal, K., Gunn, K. L., Beal, L. M., Elipot, S., & Willis, J. K. (2022). Reduction in Meridional Heat Export Contributes to Recent Indian Ocean Warming. *Journal of Physical Oceanography*, *52*(3), 329–345. https://doi.org/10.1175/JPO-D-21-0085.1

Medhaug, I., Langehaug, H. R., Eldevik, T., Furevik, T., & Bentsen, M. (2012). Mechanisms for decadal scale variability in a simulated Atlantic meridional overturning circulation. *Climate Dynamics*, *39*(1), 77–93. https://doi.org/10.1007/s00382-011-1124-z

Merrifield, M. A., Thompson, P. R., & Lander, M. (2012). Multidecadal sea level anomalies and trends in the western tropical Pacific. *Geophysical Research Letters*, *39*(13). https://doi.org/10.1029/2012GL052032

Nissan, H., Goddard, L., de Perez, E. C., Furlow, J., Baethgen, W., Thomson, M. C., & Mason, S. J. (2019). On the use and misuse of climate change projections in international development. *WIREs Climate Change*, *10*(3), e579. https://doi.org/10.1002/wcc.579

Olonscheck, D., Rugenstein, M., & Marotzke, J. (2020). Broad Consistency Between Observed and Simulated Trends in Sea Surface Temperature Patterns. *Geophysical Research Letters*, *47*(10), e2019GL086773. https://doi.org/10.1029/2019GL086773

Palmer, M. D., Bryden, H. L., Hirschi, J., & Marotzke, J. (2004). Observed changes in the South Indian Ocean gyre circulation, 1987-2002. *Geophysical Research Letters*, *31*(15), 2–5. https://doi.org/10.1029/2004GL020506

Peng, Q., Xie, S.-P., Wang, D., Huang, R. X., Chen, G., Shu, Y., Shi, J.-R., & Liu, W. (2022). Surface warming–induced global acceleration of upper ocean currents. *Science Advances*, *8*(16), eabj8394. https://doi.org/10.1126/sciadv.abj8394

Polo, I., Robson, J., Sutton, R., & Balmaseda, M. A. (2014). The Importance of Wind and Buoyancy Forcing for the Boundary Density Variations and the Geostrophic Component of the AMOC at 26°N. *Journal of Physical Oceanography*, *44*(9), 2387–2408. https://doi.org/10.1175/JPO-D-13-0264.1

Rodgers, K. B., Lee, S.-S., Rosenbloom, N., Timmermann, A., Danabasoglu, G., Deser, C., Edwards, J., Kim, J.-E., Simpson, I. R., Stein, K., Stuecker, M. F., Yamaguchi, R., Bódai, T., Chung, E.-S., Huang, L., Kim, W. M., Lamarque, J.-F., Lombardozzi, D. L., Wieder, W. R., & Yeager, S. G. (2021). Ubiquity of human-induced changes in climate variability. *Earth System Dynamics*, *12*(4), 1393–1411. https://doi.org/10.5194/esd-12-1393-2021

Roemmich, D., Gilson, J., Davis, R., Sutton, P., Wijffels, S., & Riser, S. (2007). Decadal Spinup of the South Pacific Subtropical Gyre. *Journal of Physical Oceanography*, *37*(2), 162–173. https://doi.org/10.1175/JPO3004.1

Roemmich, D., Gilson, J., Sutton, P., Zilberman, N., Roemmich, D., Gilson, J., Sutton, P., & Zilberman, N. (2016). Multidecadal Change of the South Pacific Gyre Circulation. *Journal of Physical Oceanography*, *46*(6), 1871–1883. https://doi.org/10.1175/JPO-D-15-0237.1

Rose, B. E. J., Armour, K. C., Battisti, D. S., Feldl, N., & Koll, D. D. B. (2014). The dependence of transient climate sensitivity and radiative feedbacks on the spatial pattern of ocean heat uptake. *Geophysical Research Letters*, *41*(3), 1071–1078. https://doi.org/10.1002/2013GL058955

Rugenstein, M. A. A., Winton, M., Stouffer, R. J., Griffies, S. M., & Hallberg, R. (2013). Northern high-latitude heat budget decomposition and transient warming. *Journal of Climate*, *26*(2), 609–621. https://doi.org/10.1175/JCLI-D-11-00695.1

Santer, B. D., Wigley, T. M. L., Boyle, J. S., Gaffen, D. J., Hnilo, J. J., Nychka, D., Parker, D. E., & Taylor, K. E. (2000). Statistical significance of trends and trend differences in layer-average atmospheric temperature time series. *Journal of Geophysical Research: Atmospheres*, *105*(D6), 7337–7356. https://doi.org/10.1029/1999JD901105

Seager, R., Cane, M., Henderson, N., Lee, D.-E., Abernathey, R., & Zhang, H. (2019). Strengthening tropical Pacific zonal sea surface temperature gradient consistent with rising greenhouse gases. *Nature Climate Change*, *9*(7), Article 7. https://doi.org/10.1038/s41558-019-0505-x

Seager, R., Henderson, N. L., & Cane, M. A. (2022). *Persistent discrepancies between observed and modeled trends in the tropical Pacific Ocean*. *35*(14), 4571–4584. https://doi.org/10.7916/6wd4-f378

SHI, J. R., TALLEY, L. D., XIE, S. P., LIU, W., & GILLE, S. T. (2020). Effects of buoyancy and wind forcing on southern ocean climate change. *Journal of Climate*, *33*(23), 10003–10020. https://doi.org/10.1175/JCLI-D-19-0877.1

Shi, J. R., Talley, L. D., Xie, S. P., Peng, Q., & Liu, W. (2021). Ocean warming and accelerating Southern Ocean zonal flow. *Nature Climate Change*, *11*(12), 1090–1097. https://doi.org/10.1038/s41558-021-01212-5

Smith, R., Jones, P., Briegleb, B., Bryan, F., Danabasoglu, G., Dennis, J., Dukowicz, J., Eden, C., Fox-Kemper, B., Gent, P. R., Hecht, M., Jayne, S., Jochum, M., Large, W., Lindsay, K., Maltrud, M., Norton, N., Peacock, S., Vertenstein, M., & Yeager, S. (2010). *The Parallel Ocean Program (POP) Reference Manual*.

Stevens, B., Sherwood, S. C., Bony, S., & Webb, M. J. (2016). Prospects for narrowing bounds on Earth's equilibrium climate sensitivity. *Earth's Future*, *4*(11), 512–522. https://doi.org/10.1002/2016EF000376

Thompson, D. W. J., & Solomon, S. (2002). Interpretation of Recent Southern Hemisphere Climate Change. *Science*, *296*(5569), 895–899. https://doi.org/10.1126/science.1069270

Thompson, D. W. J., Solomon, S., Kushner, P. J., England, M. H., Grise, K. M., & Karoly, D. J. (2011). Signatures of the Antarctic ozone hole in Southern Hemisphere surface climate change. *Nature Geoscience*, *4*(11), Article 11. https://doi.org/10.1038/ngeo1296

Timmermann, A., McGregor, S., & Jin, F. F. (2010). Wind effects on past and future regional sea level trends in the southern Indo-Pacific. *Journal of Climate*, *23*(16), 4429–4437. https://doi.org/10.1175/2010JCLI3519.1

Trossman, D. S., Palter, J. B., Merlis, T. M., Huang, Y., & Xia, Y. (2016). Large-scale ocean circulation-cloud interactions reduce the pace of transient climate change. *Geophysical Research Letters*, *43*(8), 3935–3943. https://doi.org/10.1002/2016GL067931

Turner, J., Bracegirdle, T. J., Phillips, T., Marshall, G. J., & Hosking, J. S. (2013). An Initial Assessment of Antarctic Sea Ice Extent in the CMIP5 Models. *Journal of Climate*, *26*(5), 1473–1484. https://doi.org/10.1175/JCLI-D-12-00068.1

Vecchi, G. A., & Soden, B. J. (2007). Global Warming and the Weakening of the Tropical Circulation. *Journal of Climate*, *20*(17), 4316–4340. https://doi.org/10.1175/JCLI4258.1

Wang, H., Xie, S.-P., & Liu, Q. (2016). Comparison of Climate Response to Anthropogenic Aerosol versus Greenhouse Gas Forcing: Distinct Patterns. *Journal of Climate*, *29*(14), 5175–5188. https://doi.org/10.1175/JCLI-D-16-0106.1

Watanabe, M., Dufresne, J.-L., Kosaka, Y., Mauritsen, T., & Tatebe, H. (2021). Enhanced warming constrained by past trends in equatorial Pacific sea surface temperature gradient. *Nature Climate Change*, *11*(1), Article 1. https://doi.org/10.1038/s41558-020-00933-3

Weijer, W., Cheng, W., Garuba, O. A., Hu, A., & Nadiga, B. T. (2020). CMIP6 Models Predict Significant 21st Century Decline of the Atlantic Meridional Overturning Circulation. *Geophysical Research Letters*, *47*(12), e2019GL086075. https://doi.org/10.1029/2019GL086075

Winton, M., Griffies, S. M., Samuels, B. L., Sarmiento, J. L., & Frölicher, T. L. (2013). Connecting Changing Ocean Circulation with Changing Climate. *Journal of Climate*, *26*(7), 2268–2278. https://doi.org/10.1175/JCLI-D-12-00296.1

Xie, S.-P., Lu, B., & Xiang, B. (2013). Similar spatial patterns of climate responses to aerosol and greenhouse gas changes. *Nature Geoscience*, *6*(10), 828–832. https://doi.org/10.1038/ngeo1931

Yeager, S., & Danabasoglu, G. (2014). The Origins of Late-Twentieth-Century Variations in the Large-Scale North Atlantic Circulation. *Journal of Climate*, *27*(9), 3222–3247. https://doi.org/10.1175/JCLI-D-13-00125.1

Zhou, C., Zelinka, M. D., & Klein, S. A. (2017). Analyzing the dependence of global cloud feedback on the spatial pattern of sea surface temperature change with a Green's function approach. *Journal of Advances in Modeling Earth Systems*, *9*(5), 2174–2189. https://doi.org/10.1002/2017MS001096

Geophysical Research Letters

Supporting Information for

Historical changes in wind driven ocean circulation can accelerate global warming

Kay McMonigal[1], Sarah Larson[1], Shineng Hu[2], and Ryan Kramer[3,4]

[1] Department of Marine, Earth, and Atmospheric Sciences, North Carolina State University, Raleigh, NC, USA

[2] Division of Earth and Climate Sciences, Nicholas School of the Environment, Duke University, Durham, NC, USA

[3] Climate and Radiation Laboratory, Earth Sciences Division, NASA Goddard Space Flight Center, Greenbelt, MD, USA
[4] Goddard Earth Science Technology Research II, University of Maryland Baltimore County, Baltimore, MD, USA

Corresponding author: Kay McMonigal (ktmcmoni@ncsu.edu)

Contents of this file

Figures S1 to S10
Table S1

Introduction

This file contains ten figures and one table as supporting information for "Historical changes in wind driven ocean circulation can accelerate global warming".

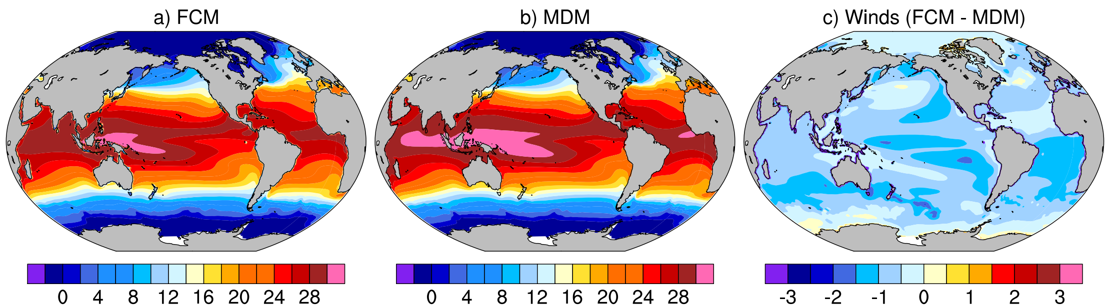

Figure S1: Pre industrial time mean sea surface temperature in a) FCM, b) MDM, and c) FCM – MDM. Units are °C.

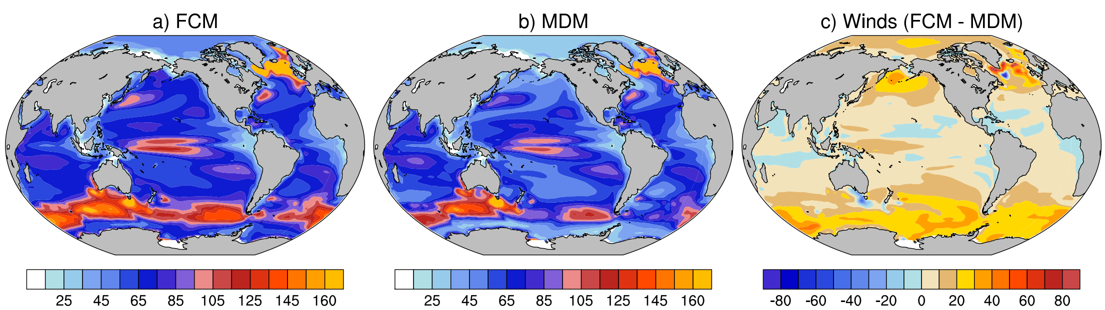

Figure S2: Pre industrial time mean mixed layer depth in a) FCM, b) MDM, and c) FCM – MDM. Units are meters.

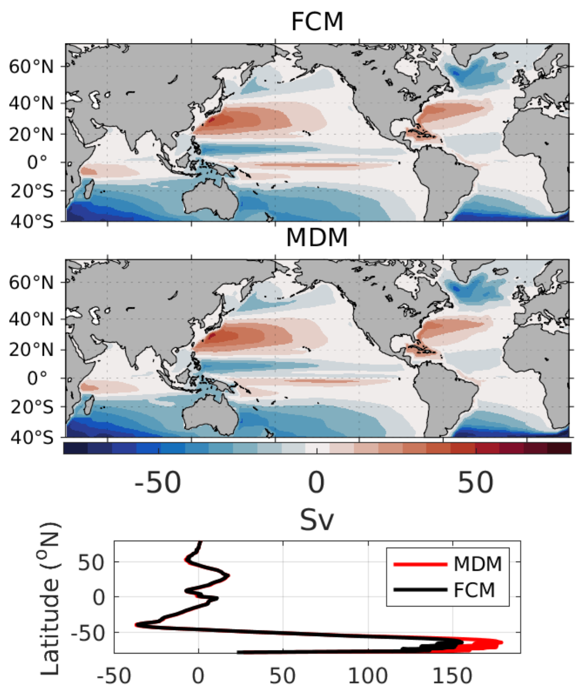

Figure S3: Pre industrial, annual mean barotropic stream function (BSF) in the FCM and MDM CESM2 simulations. The bottom panel shows the zonally averaged BSF. Units are Sverdrups (Sv). Positive values indicate clockwise flow in the x,y-plane and negative values indicate counterclockwise flow.

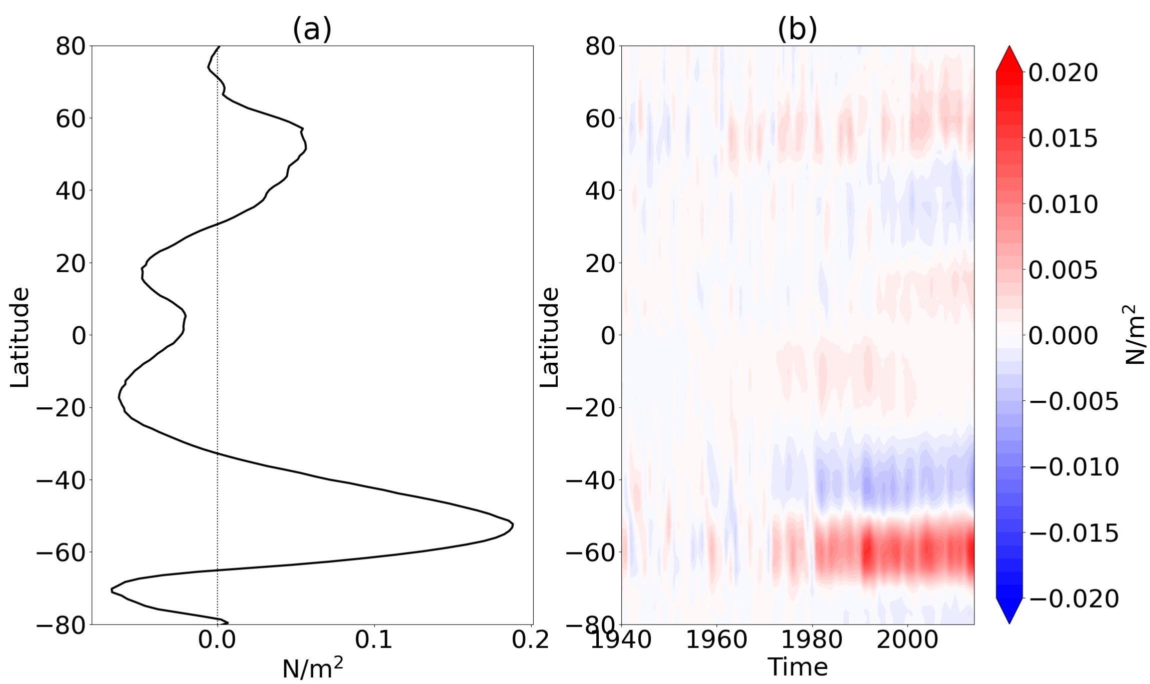

Figure S4. (a) 1941-1970 mean zonal mean wind stress in FCM ensemble mean. (b) Hovmoller plot of zonal wind stress changes relative to 1941-1970 in FCM ensemble mean.

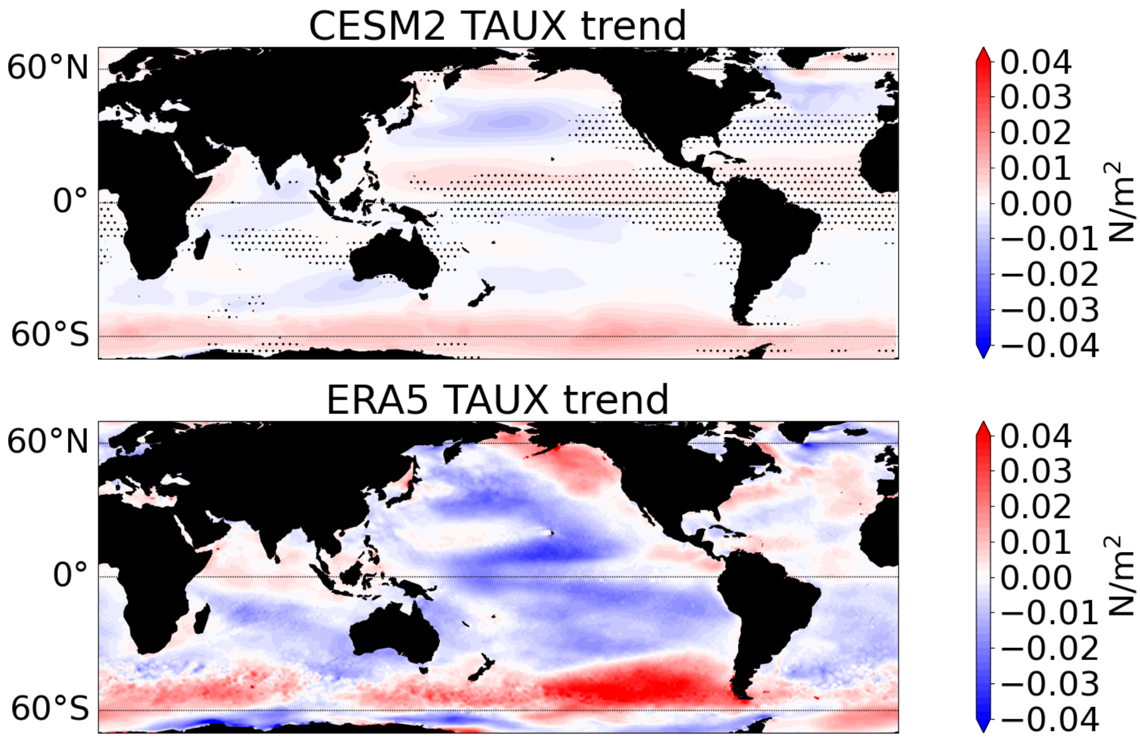

Figure S5. (top) Ensemble mean 1979-2014 trend in zonal wind stress from the FCM experiment with stippling showing where observations are outside of the range of model ensemble members. (bottom) ERA5 1979-2014 trend in zonal wind stress.

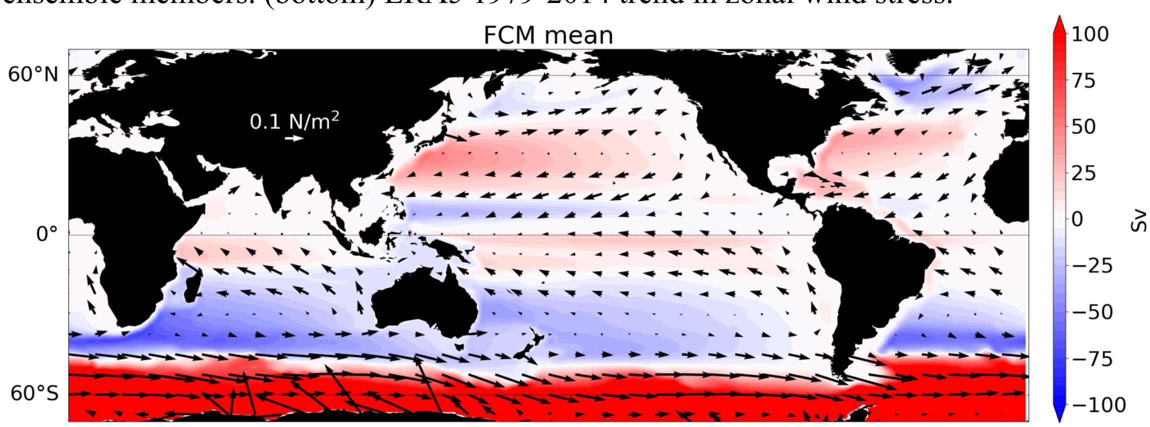

Figure S6. 1941-1970 mean BSF (colors) and wind stress (arrows) in FCM.

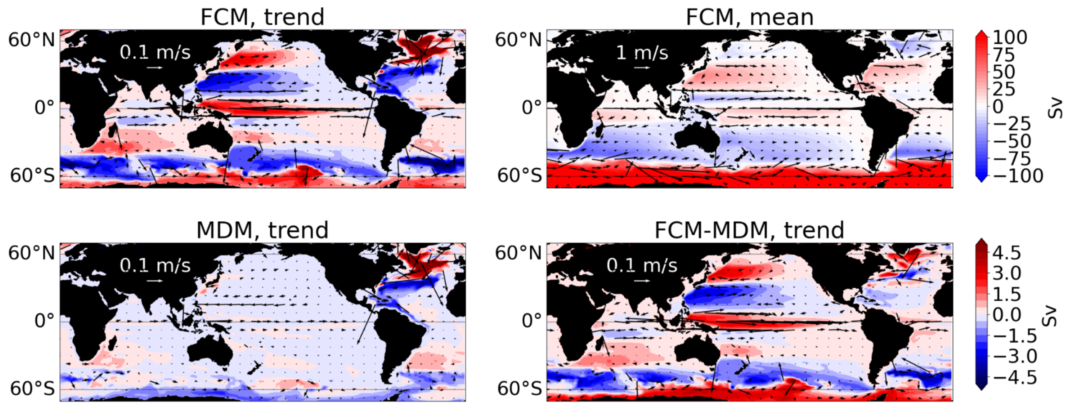

Figure S7. Comparison of barotropic streamfunction (colors) and upper 150 m ocean currents (arrows) for (top left) FCM trend over 1979-2014, (top right) FCM time mean over 1850-2014, (bottom left) MDM trend over 1979-2014, and (bottom right) FCM minus MDM trend over 1979-2014. Positive values of the barotropic streamfunction denote clockwise, negatives denote counterclockwise.

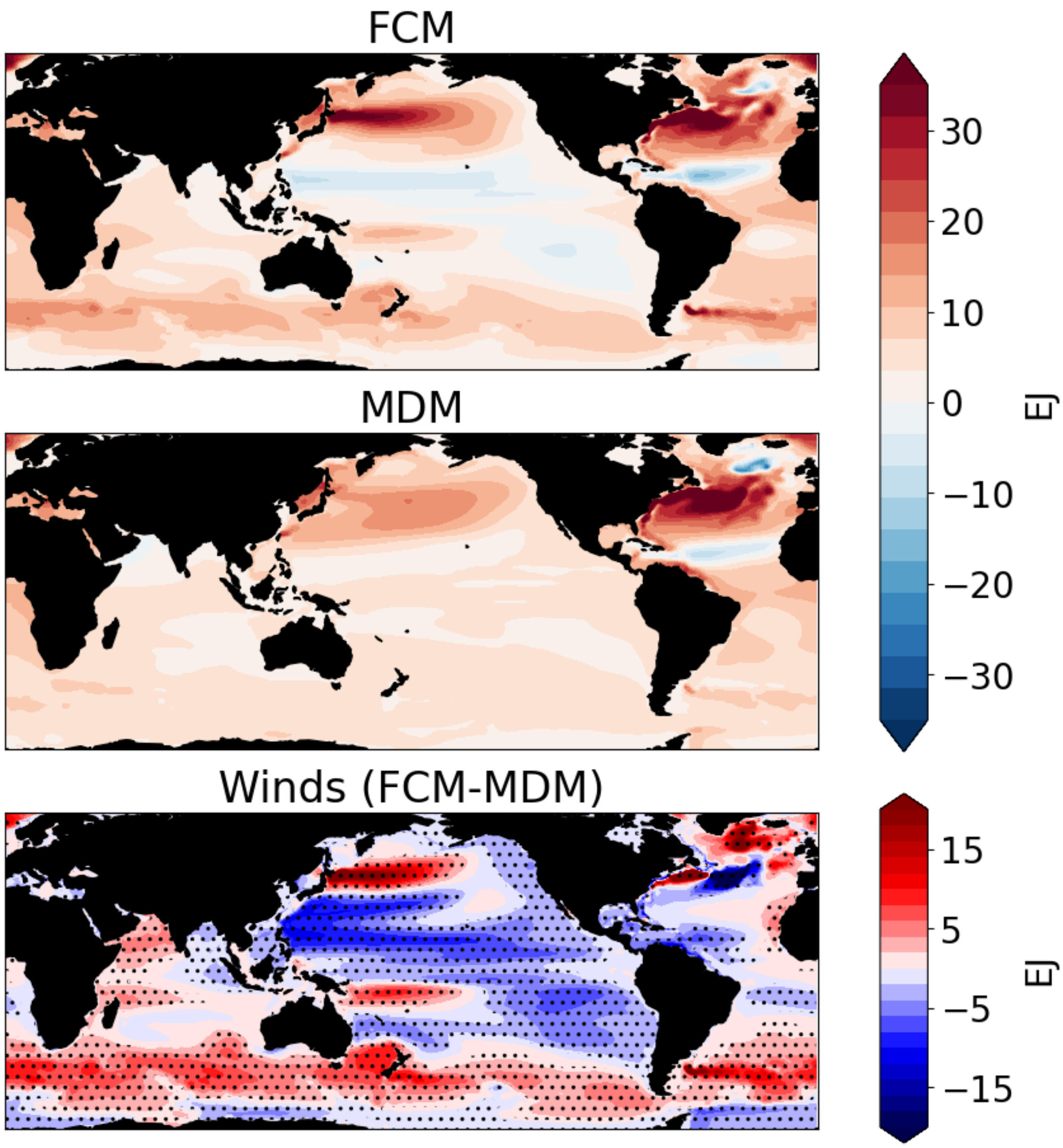

Figure S8. Ensemble mean 0-2000 m ocean heat content trend over 1979-2014

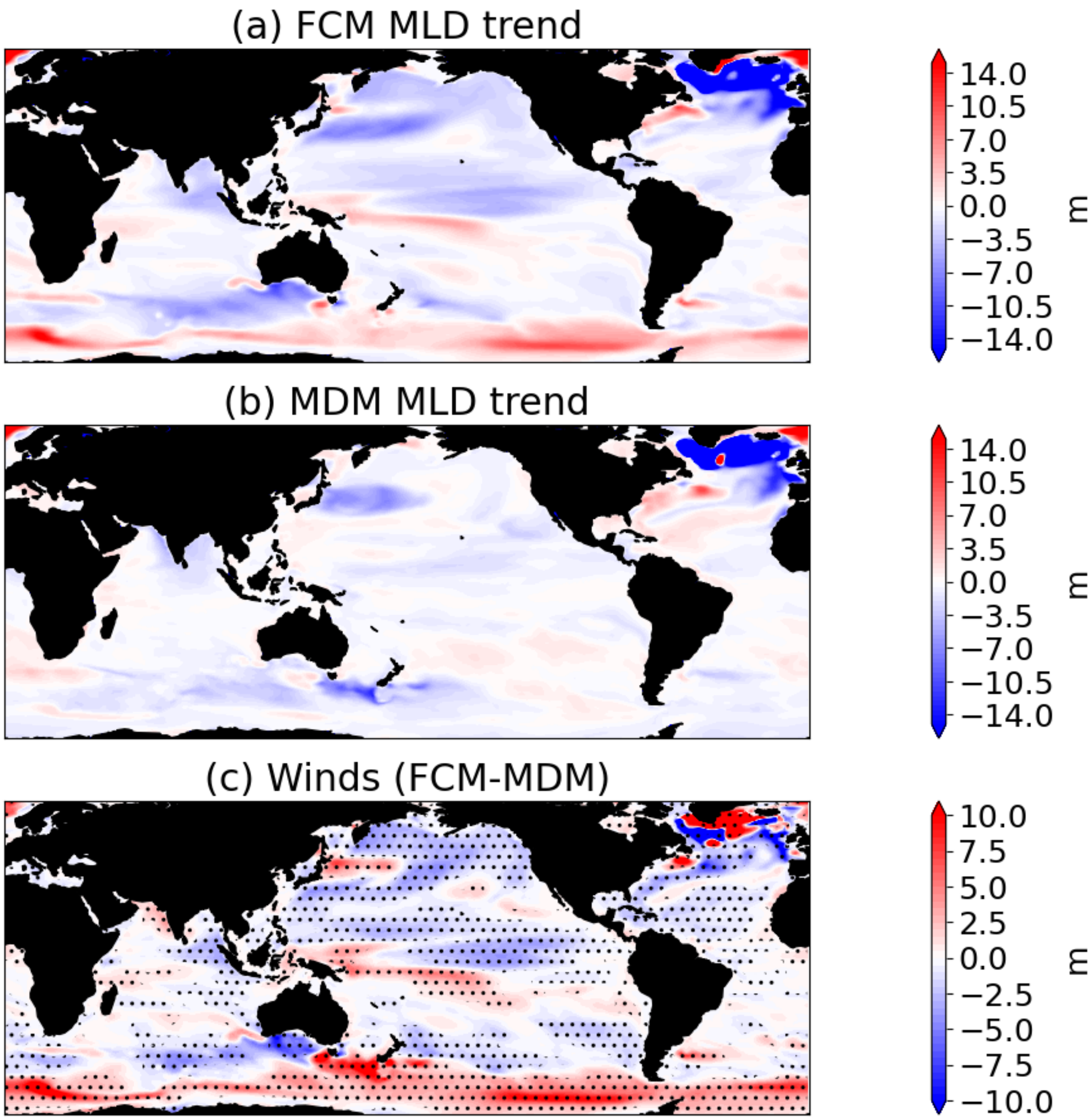

Figure S9. Mixed layer depth trend over 1979-2014 in (a) FCM ensemble mean (b) MDM ensemble mean (c) FCM-MDM.

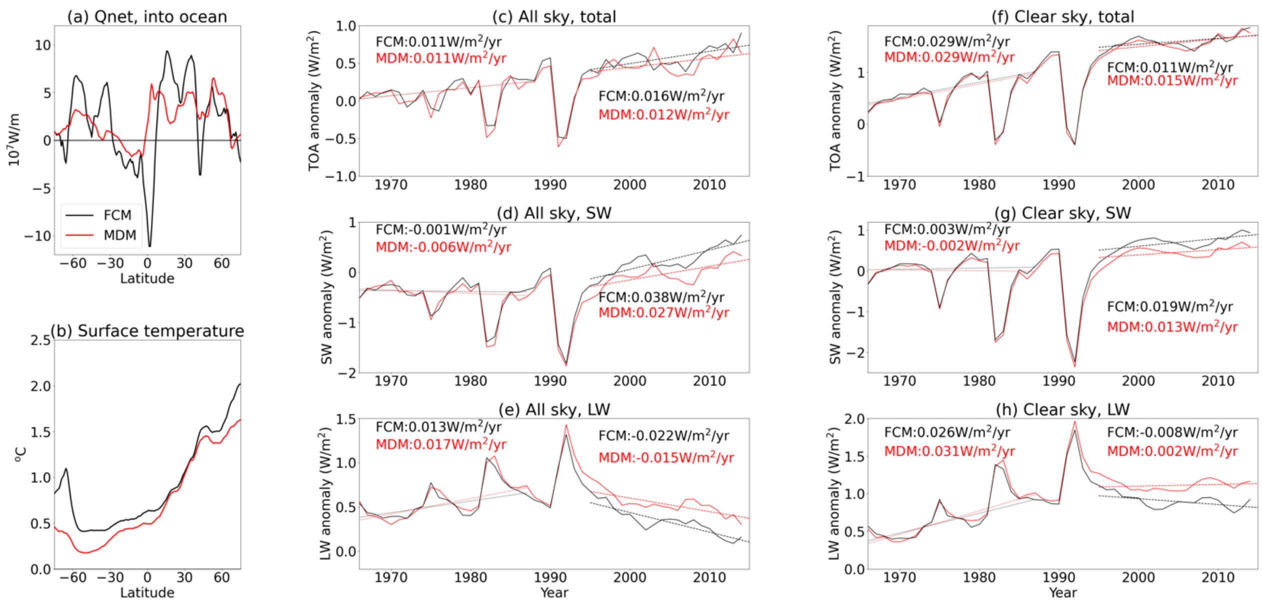

Figure S10. Ensemble mean 1979-2014 trends in zonally averaged (a) Qnet and (b) surface air temperature as a function of latitude. FCM is the black line and MDM is the red line. (c-h) Top of atmosphere radiation anomalies relative to 1941-1970, with regression line slopes. Black solid lines are FCM ensemble means, red solid lines are MDM ensemble means. Black and red dotted lines are the linear trends over 1966-1987, excluding 1975, 1982, and 1983, from FCM and MDM respectively. Black and red dashed lines are the linear trends over 1996-2014 from FCM and MDM respectively. All radiation values are defined as positive downward.

	FCM ensemble mean	MDM ensemble mean
Ocean heat uptake (W/m^2)	0.751	0.695
Warming (K)	0.847	0.699
Ocean heat uptake efficiency ($W/m^2/K$)	0.89	0.99

Table S1. Ocean heat uptake, surface air temperature warming, and ocean heat uptake efficiency (defined as ocean heat uptake/surface air temperature warming) over 1979-2014.